Conference Paper

Aerial Forest Fire Detection and Monitoring Using a Small UAV

Joaquim Vasconcelos Reinolds de Sousa and Pedro Vieira Gamboa

University of Beira Interior

Corresponding Author:
Joaquim Vasconcelos Reinolds
de Sousa
joaquimsousa91@sapo.pt

Abstract

In recent years, large patches of forest have been destroyed by fires, bringing tragic consequences for the environment and small settlements established around these regions. In this context, it is essential that fire fighting teams possess an increased situational awareness about the fire propagation, in order to promptly act in the extinguishing process. Recent advances in UAV technology allied with remote sensing and computer vision techniques show very promising UAVs applicability in forest fires detection and monitoring. Besides presenting lower operational costs, these vehicles are able to reach regions that are inaccessible or considered too dangerous for fire fighting crews operations. This paper describes the application of a real-time forest fire detection algorithm using aerial images captured by a video camera onboard an Unmanned Aerial Vehicle (UAV). The forest fire detection algorithm consists of a rule-based colour model that uses both RGB and YCbCr colour spaces to identify fire pixels. An intuitive targeting system was also developed, allowing the detection of multiple fires at the same time. Additionally, a fire geolocation algorithm was developed in order to estimate the fire location in terms of latitude (φ), longitude (λ) and altitude (h). The geolocation algorithm consists of applying two coordinates systems transformations between the body-fixed frame, North-East-Down frame (NED) and Earth-Centered, Earth Fixed (ECEF) frame. Flight tests were performed during a controlled burn in order to assess the fire detection algorithm performance. The algorithm was able to detect the fire with few false positive detections.

1. Introduction

In recent years, there has been a significant incidence of forest fires, responsible for devastating millions of forest hectares [1]. Besides destroying the local flora and fauna, these fires also destroy several infrastructures and unfortunately cause human casualties among the fire fighting crews and civilians that might be accidentally surrounded by the fire. Thus, early detection and real-time fire perception are two key factors that allow the fire fighting crews to act accordingly in order to prevent the fire from achieving unmanageable proportions [2]. Recent advances in Unmanned

Aerial Vehicles (UAV) technology allied with Remote Sensing Techniques, show very promising UAV applications in forest fires detection and monitoring [3]. This technology can provide a broader and more accurate perception of the fire, even in regions that are inaccessible or considered too dangerous for fire fighting crews operations [4]. Additionally, the operating cost of UAVs is considerably lower when compared to the currently used solutions [5].

The current fire detection methods consist of applying image processing techniques to onboard visual and infrared sensors data [6]. These techniques use characteristic features such as colour, motion, and geometry to detect the flame or smoke generated by the fire [1], [7]–[13].

Israeli Aircraft Industries developed a UAV equipped with both visible spectrum and Forward- looking infrared (FLIR) cameras. Both sensors data were processed to provide information about the geometric characteristics of the fire [14]. Martínez-de Dios et al. [15] and Pastor et al. [16] used a rotary-wing UAV also equipped with a visual and infrared camera. Each camera data are processed individually and then merged using statistical data fusion techniques.

Several studies are now focused on using a team of UAVs, characterized by increased autonomy and group cooperative behaviours for accomplishing a common task [17–21].

This paper describes the implementation of a fire segmentation algorithm in order to perform aerial forest fire detection and monitoring using a small UAV. The fire pixel segmentation algorithm is based on the work developed by Vipin et al. [12] and consists of a rule-based colour model. This algorithm requires low computational power allowing a small UAV, equipped with a visual camera and an onboard computer, to perform real-time forest fire detection. A commercial off-the-shelf multicopter, the DJI F550 hexacopter, was used as a test platform to assess the fire detection and monitoring effectiveness. Several flight tests, conducted on a real fire scenario, showed that the UAV is capable of successfully detecting a forest fire.

2. Fire Detection and Monitoring Algorithm

2.1. Fire Pixel Segmentation

The fire segmentation technique is based on the work developed by Vipin et al. [12] and consists of applying a set of rules to each pixel of the live video feed captured by the onboard camera. This algorithm uses both RGB (Red, Green and Blue) and YCbCr (Luminance, Chrominance blue and Chrominance Red) colour spaces. A colour space is

an abstract mathematical model that relates numbers to actual colours, allowing several devices to represent a colour in a digital environment.

The RGB is an additive colour space defined by the combination of three colour planes: red, green and blue. Each component value ranges from 0 to 255. For instance, the red colour is represented by (R,G,B) = (255,0,0), green by (R,G,B) = (0,255,0) and blue by (R,G,B) = (0,0,255).

In the YCbCr colour space, the intensity and chrominance are well discriminated, where Y is the luminance, Cb and Cr are the chrominance blue and red components respectively. The luminance (Y component) measures the light intensity while the chrominance (Cb and Cr components) measures the colour values [22].

The fire pixel segmentation algorithm consists of a set of seven colour-based rules applied to each frame of the live video feed. All rules must be met in order to categorise a pixel as fire.

2.1.1. Rule I

Considering that each video frame consists of a rectangular grid of *M×N* pixels, each pixel location is given by (*x,y*), being *R(x,y)*, *G(x,y)* and *B(x,y)* the corresponding intensity values of red, green and blue channels, respectively. Rule I states that in fire regions, the red channel intensity is higher than the green channel. Moreover, the green channel intensity is higher than the blue channel. Thus, for a pixel located at (*x,y*) position to become a fire pixel, the following condition must be met:

$$R(x, y) > G(x, y) > B(x, y) \tag{1}$$

2.1.2. Rule II

Rule II specifies the threshold values for each RGB channel from which a pixel can be considered as fire. Vipin et al. [12] identified this threshold by analysing the histogram of a large number of fire images. According to their observation, a pixel located at (*x,y*) position is considered fire when the following condition is met:

$$R(x, y) > 190 \cap G(x, y) > 100 \cap B(x, y) < 140 \tag{2}$$

2.1.3. Rule III

Rule III states that a fire pixel exhibits a higher luminance (Y) value when compared to the chrominance blue component (Cb), thus:

$$Y(x, y) \geq C_b(x, y) \tag{3}$$

Each component value of the YCbCr colour space can be calculated using the following RGB to YCbCr conversion:

$$
\begin{bmatrix} Y(x, y) \\ C_b(x, y) \\ C_r(x, y) \end{bmatrix} = \begin{bmatrix} 0.2568 & 0.5041 & 0.0979 \\ -0.1482 & -0.2910 & 0.4392 \\ 0.4392 & -0.3678 & -0.0714 \end{bmatrix} \begin{bmatrix} R(x, y) \\ G(x, y) \\ B(x, y) \end{bmatrix} + \begin{bmatrix} 16 \\ 128 \\ 128 \end{bmatrix} \tag{4}
$$

2.1.4. Rule IV

Rule IV establishes a comparison between both chrominance values of the YCbCr colour space. It states that for a fire pixel the chrominance red values prevail over the chrominance blue values:

$$C_r(x, y) \geq C_b(x, y) \tag{5}$$

2.1.5. Rule V

Rule V compares each pixel YCbCr channel value with the overall image mean values of each channel. Vipin et al. [12] observed that for the flame region, the Y component, in essence the brightness, is more prominent than the mean Y component (Y_{mean}) of the overall image. Similarly, the Cb component is generally smaller than the mean Cb value of the overall image while the Cr component is higher than the overall image Cr_{mean}:

$$Y(x, y) \geq Y_{mean} \cap C_b(x, y) \leq C_{b_{mean}} \cap C_r(x, y) \geq C_{r_{mean}} \tag{6}$$

The mean values of each channel of the YCbCr colour space are calculated as follows:

$$Y_{mean} = \frac{1}{MN} \sum_{x=1}^{M} \sum_{y=1}^{N} Y(x, y) \tag{7}$$

$$C_{b_{mean}} = \frac{1}{MN} \sum_{x=1}^{M} \sum_{y=1}^{N} C_b(x, y) \tag{8}$$

$$C_{r_{mean}} = \frac{1}{MN} \sum_{x=1}^{M} \sum_{y=1}^{N} C_r(x, y) \tag{9}$$

2.1.6. Rule VI

Vipin et al. [12] observed a significant difference between the *Cb* and *Cr* components of fire pixels. This difference results in Rule VI that states that for a fire pixel, the difference between the *Cb* and *Cr* components must be equal or higher than a given threshold:

$$|C_b - C_r| \geq Th \tag{10}$$

The threshold value (*Th*) is determined according to the Receiver Operating Characteristics (ROC) curve exhibited in Figure 1. This curve is created by plotting the True Positive Rate (TPR) against the False Positive Rate (FPR) at different threshold values. The True Positive Rate (TPR) is the ratio between true positive fire detections and the number of test images that actually contained a fire region. The False Positive Rate (FPR) is the ratio between the number of false positive fire detections and the number of test images containing no fire. According to Figure 1, point C exhibits the best balance between high true positives (>95%) and low false positives (<30%) with a corresponding threshold value of *Th* = 70.

2.1.7. Rule VII

Rule VII applies the same principle as Rule II. It specifies the threshold values for both *Cb* and *Cr* channels from which a pixel can be considered as fire. The luminance component (*Y*) is not considered because it is highly dependent on illumination conditions. Rule VII states that a pixel located at (*x,y*) position is considered fire when the following condition is met:

$$C_b(x, y) \leq 120 \cap C_r(x, y) \geq 150 \tag{11}$$

Figure 2 exhibits the resulting binary image after applying the aforementioned rules to an aerial image of a real fire.

Besides performing an effective fire detection, the binary image is not suitable for a real operational scenario. In the present work, a more intuitive mean of fire identification, consisting of a targeting system, was developed to assess this necessity. Additionally, due to the possibility of having multiple ongoing fires in the camera Field of View (FOV), the rectangular pixels grid was divided into multiple rectangular sectors, each one comprising an independent targeting system.
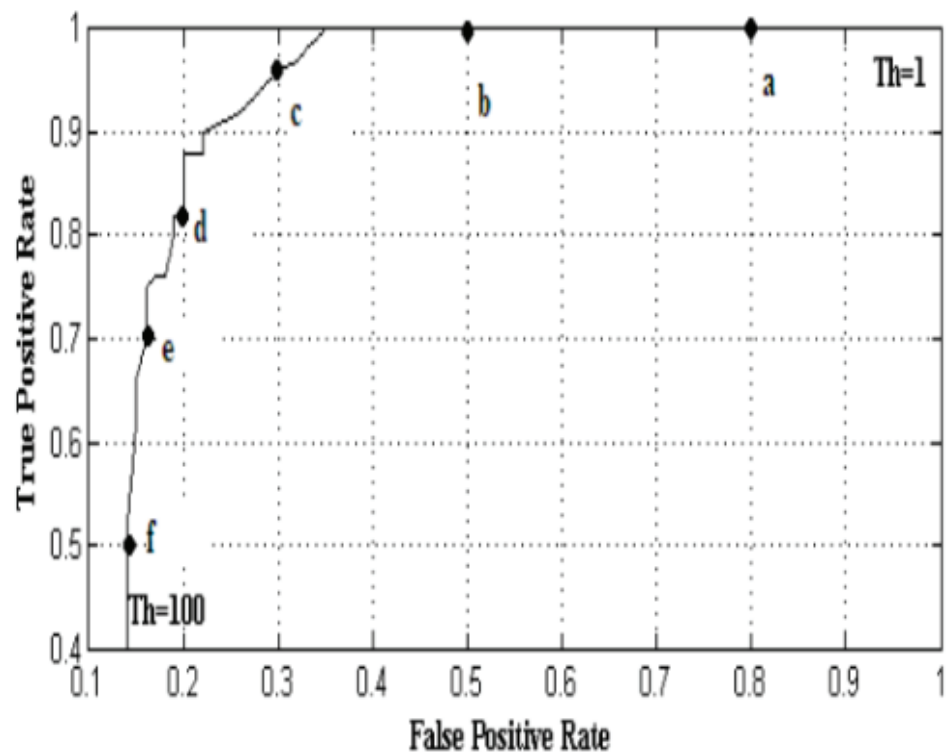
Figure 1: Receiver Operating Characteristics (ROC) curve Source: [13]
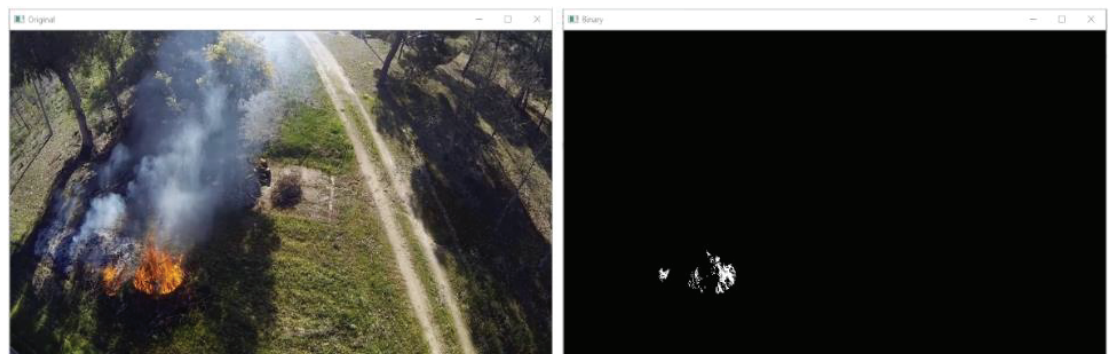
Figure 2: Non-processed fire aerial image (left) and binary image (right) after applying the fire pixel segmentation rules (Source: Author).

Figure 3 displays the targeting system overlayed on the live video feed captured by the onboard camera. This system consists of a blue diamond-shaped symbol and a green square.

The blue diamond-shaped symbol represents the centroid of the fire pixel cluster. The centroid, *C(x,y)*, is calculated in each frame of the video feed, and it is given by:

$$C(x, y) = \left(\frac{\sum_{i=1}^{T} x_i}{T}, \frac{\sum_{i=1}^{T} y_i}{T} \right)$$

(12)

Figure 3: Fire detection and monitoring targeting system (Source: Author).

where T is the total number of fire pixels detected in each video frame, x_i and y_i are the coordinates of each fire pixel on the $M{\times}N$ rectangular pixels grid.

Due to the flickering motion of the flames, the position of the fire pixels centroid keeps continually changing at the same framerate as the video feed, causing some difficulties when tracking the blue diamond-shaped symbol. Therefore, a Kalman filter [23] was applied, providing a smoother and more intuitive way of tracking the fire position. The green square represents the current Kalman filter estimate using the previous frames centroids as inputs.

2.2. Fire Geolocation

The fire geolocation must be precisely known by fire fighting crews in order to promptly and effectively act during the extinction process.

The fire geolocation can be estimated by knowing the UAV position and attitude, and the distance between the UAV and the fire itself.

The UAV position in terms of latitude (φ), longitude (λ) and altitude (h), is given by the autopilot NAZA-M V2, based on the Global Positioning System (GPS) signal. The autopilot also provides the three Euler angles, pitch (θ), roll (ϕ,) and yaw (ψ), required to define the UAV attitude.

The distance between the UAV and the fire, from now on referred as detection distance (L_{det}), is measured by a Light Detection and Ranging (LIDAR) sensor. The LIDAR

beam, as well as the onboard visual camera, are assumed to be positioned at the UAV centre of mass, aligned with the vertical body axis (z_B), as shown in Figure 4. Consequently, the fire location, F_B, in the UAV body-fixed frame is (0,0,L_{det}).
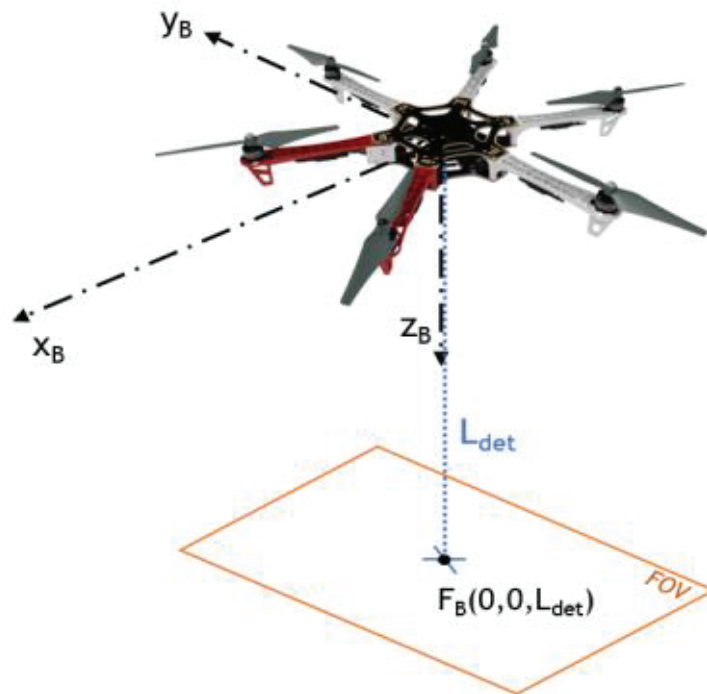
**Figure** 4: UAV body-fixed frame (Source: Author).

In order to estimate the fire geodetic coordinates (latitude, longitude and height), a series of transformations between different coordinate systems are required [24].

The first step consists of transforming the fire location from the UAV body-fixed frame to the North-East-Down frame (NED). The NED system has its origin on the surface of the geoid below the aircraft's centre of mass, being the *x*-axis oriented to north, the *y*-axis oriented to east and the *z*-axis oriented down. This transformation uses the three Euler angles (θ, ϕ, ψ) and is performed through the rotation matrix (R_{B_NED}), as follows:

$$F_{NED} = R_{B\_NED} \cdot F_B \tag{13}$$

$$
\begin{bmatrix} x_{NED} \\ y_{NED} \\ z_{NED} \end{bmatrix}
$$

$$
= \begin{bmatrix} \cos\psi\cos\theta & \cos\psi\sin\theta\sin\phi - \sin\psi\cos\phi & \cos\psi\sin\theta\cos\phi + \sin\psi\sin\phi \\ \sin\psi\cos\theta & \sin\psi\sin\theta\sin\phi + \cos\psi\cos\phi & \sin\psi\sin\theta\cos\phi - \cos\psi\sin\phi \\ -\sin\theta & \cos\theta\sin\phi & \cos\theta\cos\phi \end{bmatrix} \begin{bmatrix} x_B \\ y_B \\ z_B \end{bmatrix}
$$

(14)
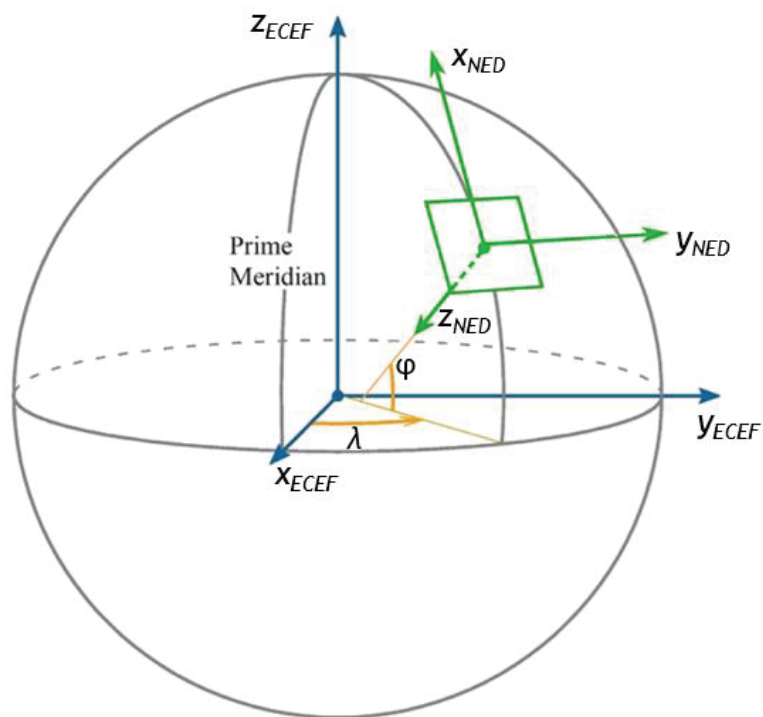
Figure 5: NED (green) and ECEF (blue) coordinates systems (Source: [25]).

The next step results from the transformation of the fire location in the NED frame to the Earth-Centered, Earth Fixed (ECEF) frame. The ECEF is a cartesian coordinate system with the origin fixed at the Earth's centre of mass. The x-axis points towards the intersection of Earth's equatorial plane and the Greenwich Meridian, the *y*-axis points 90 degrees to the east of the *x*-axis in the equatorial plane, and the *z*-axis points northward along the Earth's rotation axis [25]. Figure 5 exhibits a graphical representation of both the NED and ECEF coordinate systems.

The transformation from NED to ECEF coordinates systems is given by:

$$
F_{ECEF} = R_{NED\_ECEF} \cdot F_{NED} + P_{ref\_ECEF}
$$

(15)

where, P_{ref_ECEF} is the UAV position in the ECEF coordinates system, and the rotation matrix (R_{NED_ECEF}) is given by:

$$R_{NED\_ECEF} = \begin{bmatrix} -\sin\psi\cos\lambda & -\sin\lambda & -\cos\psi\cos\lambda \\ -\sin\psi\sin\lambda & \cos\lambda & -\cos\psi\sin\lambda \\ \cos\psi & 0 & -\sin\psi \end{bmatrix} \tag{16}$$

The UAV position is provided by the autopilot in geodetic coordinates (latitude, longitude, height), so it first must be converted to ECEF coordinates (x_{ECEF}, y_{ECEF}, z_{ECEF}) according to the World Geodetic System, WGS-84, using the following equations:

$$x_{ECEF} = (N(\psi) + h)\cos\psi\cos\lambda \tag{17}$$

$$y_{ECEF} = (N(\psi) + h)\cos\psi\sin\lambda \tag{18}$$

$$z_{ECEF} = \left(\frac{b^2}{a^2}N(\psi) + h\right)\cos\psi\sin\lambda \tag{19}$$

where, a = 6378137 m is the earth equatorial radius, b = 6356752.3142 m is the polar radius, and $N(\varphi)$ is the prime vertical radius of curvature given by:

$$N(\psi) = \frac{a^2}{\sqrt{a^2\cos^2\psi + b^2\sin^2\psi}} \tag{20}$$

The last step consists of transforming the fire location in ECEF coordinates (F_{ECEF}) to geodetic coordinates. This transformation was achieved using the analytical method developed by Vermeille et al. [26].

3. UAV Sensors Package

The DJI F550 is a commercial off-the-shelf multicopter equipped with the NAZA-M V2 autopilot system. The autopilot comprises an internal 3-axis gyro and accelerometer, and an external GPS/compass module [27]. Figure 6 displays a simplified architecture of the avionics system.

All components placed inside the blue box are related to the Multicopter Control System. It comprises the autopilot board (NAZA-M V2), the Radio Control (RC) receiver, and the Controller Area Network (CAN) hub that establishes the communication between the autopilot board and other peripheric systems such as the GPS/Compass module, the 2-axis First Person View (FPV) camera stabiliser and the iOSD. The iOSD is an Onscreen Display module responsible for overlaying the flight data on the video signal

captured by the FPV camera. The FPV video is then transmitted to a Ground Control Station (GCS), allowing the pilot to control the UAV.

The orange box encompasses all the components related to the Fire Detection and Monitoring System. It includes a CAN transceiver, two Teensy 3.2 microcontrollers, a LIDAR, a Raspberry Pi 3B computer, and an 8-megapixel camera module. The Teensy microcontroller board 1, is connected through a CAN transceiver to the CAN hub of the Multicopter Control System. Its primary function is to decode the autopilot CAN messages that contain information about the UAV position (φ, λ, h) and attitude (ϕ, θ, ψ), and send it over the serial port to the Teensy microcontroller board 2. The LIDAR measures the detecting distance (L_{det}) and sends this information via Pulse-Width Modulation (PWM) to the Teensy microcontroller board 2. The computation of the fire geolocation is performed by the Teensy microcontroller board 2. This board gathers all data about UAV position, attitude and fire detection distance, in order to compute the fire location and send it to the Raspberry Pi via I2C communication. The Raspberry Pi computer hosts the Fire Pixel Segmentation algorithm. It processes the video signal from the 8-megapixel camera and stores the processed video signal in a miniSD flash memory card.
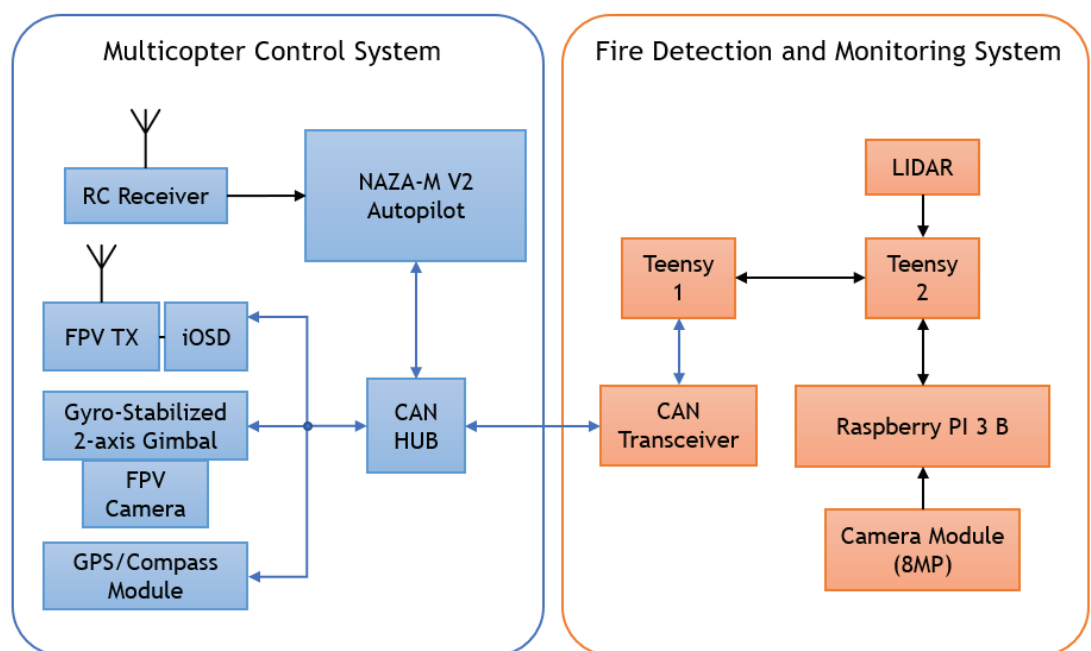
Figure 6: Avionics System simplified architecture (Source: Author).

4. UAV Flight Test and results

The flight tests were carried out during a controlled burn at 10:00 AM (UTC) of 15 March 2019, following the safety regulations issued by the civil aviation authority and civil protection agency. The test site is located at 40°14'39.0"N 7°24'01.8"W.

The UAV was manually flown in a creeping line search pattern at different heights above the fire location (Figure 7). Figure 8 displays two frames of the onboard processed video at two different flight altitudes.

The Fire Detection and Monitoring algorithm proved to be able to correctly identify the fire regions. As expected, there were a few false positive detections that occurred mainly due to the presence of man-made objects within the same fire colour range, such as the orange terracotta roof tiles of a nearby building.

Due to the limited processing power of the onboard computer (Raspberry PI 3 B), the input video had to be downsized by a factor of 2, resulting in a total resolution of 4 MP. In these conditions, the Raspberry was able to process the input video at a framerate of approximately 6 fps.

Figure 7: Flight testing during a controlled burn (Source: Author).

Figure 8: Fire Detection and Monitoring algorithm onboard processed outputs (Source: Author).

5. Conclusion

The results obtained with the present work showed that the Fire Detection and Monitoring algorithm is able to perform a real-time fire detection and monitoring using the UAV onboard footage.

Due to the limited processing power of the onboard computer, the maximum achievable output framerate was approximately 6 fps. The output framerate can be increased by downsizing the video input resolution at the expense of a lower detection range. A lower video resolution would compromise the ability to detect small fires at long distances.

Further flight tests shall be conducted in order to validate the Fire Geolocation algorithm and to quantify the effectiveness of the Fire Detection and Monitoring algorithm in terms of fire detection range.

Acknowledgments

References

[1] J. R. Martinez-de Dios, B. C. Arrue, A. Ollero, L. Merino, and F. Gómez-Rodríguez, "Computer vision techniques for forest fire perception," *Image Vis. Comput.*, vol. 26, no. 4, pp. 550–562, 2008.

[2] M. A. Akhloufi, N. A. Castro, A. Couturier, M. A. Akhloufi, N. A. Castro, and A. Couturier, "UAVs for wildland fires," in *Autonomous Systems: Sensors, Vehicles, Security, and the Internet of Everything*, 2018, vol. 10643, no. May, pp. 1–14.

[3] C. Yuan, Z. Liu, and Y. Zhang, "Fire Detection Using Infrared Images for UAV-based Forest Fire Surveillance," in *2017 International Conference on Unmanned Aircraft Systems, ICUAS 2017*, 2017, pp. 567–572.

[4] L. Zhang, B. Wang, W. Peng, C. Li, Z. Lu, and Y. Guo, "Forest fire detection solution based on UAV aerial data," Int. J. Smart Home, vol. 9, no. 8, pp. 239–250, 2015.

[5] B. R. Christensen, "Use of UAV or remotely piloted aircraft and forward-looking infrared in forest, rural and wildland fire management: evaluation using simple economic analysis," New Zeal. J. For. Sci., vol. 45, no. 1, 2015.

[6] C. Yuan, Y. Zhang, and Z. Liu, "A survey on technologies for automatic forest fire monitoring, detection, and fighting using unmanned aerial vehicles and remote sensing techniques," Can. J. For. Res., vol. 45, no. 7, pp. 783–792, 2015.

[7] P. Chamoso, A. González-Briones, F. De La Prieta, and J. M. Corchado, "Computer vision system for fire detection and report using UAVs," in Robust Solutions for Fire Fighting (RSFF'18), 2018, vol. 2146, pp. 40–49.

[8] S. Ma, Y. Zhang, J. Xin, Y. Yi, D. Liu, and H. Liu, "An Early Forest Fire Detection Method Based on Unmanned Aerial Vehicle Vision," in Proceedings of the 30th Chinese Control and Decision Conference, CCDC 2018, 2018, pp. 6344–6349.

[9] C. Yuan, Z. Liu, and Y. Zhang, "Learning-Based Smoke Detection for Unmanned Aerial Vehicles Applied to Forest Fire Surveillance," J. Intell. Robot. Syst. Theory Appl., pp. 1–13, 2018.

[10] C. Yuan, Z. Liu, and Y. Zhang, "Aerial Images-Based Forest Fire Detection for Firefighting Using Optical Remote Sensing Techniques and Unmanned Aerial Vehicles," J. Intell. Robot. Syst. Theory Appl., vol. 88, no. 2–4, pp. 635–654, 2017.

[11] C. Yuan, Z. Liu, and Y. Zhang, "Vision-based forest fire detection in aerial images for firefighting using UAVs," 2016 Int. Conf. Unmanned Aircr. Syst. ICUAS 2016, pp. 1200– 1205, 2016.

[12] C. E. Premal and S. S. Vinsley, "Image Processing Based Forest Fire Detection," Int. J. Emerg. Technol. Adv. Eng., vol. 2, no. 2, pp. 87–95, 2014.

[13] H. Cruz, M. Eckert, J. Meneses, and J. F. Martínez, "Efficient forest fire detection index for application in Unmanned Aerial Systems (UASs)," Sensors, vol. 16, no. 6, 2016.

[14] G. F. M. Center(GFMC), "Firebird 2001 Fire Fighting Management Support System," 2001..

[15] J. R. M. de Dios, L. Merino, F. Caballero, and A. Ollero, "Automatic forest-fire measuring using ground stations and unmanned aerial systems," Sensors, vol. 11, no. 6, pp. 6328–6353, 2011.

[16] E. Pastor, C. Barrado, P. Royo, E. Santamaria, J. Lopez, and E. Salami, "Architecture for a helicopter-based unmanned aerial systems wildfire surveillance system," Geocarto Int., vol. 26, no. 2, pp. 113–131, 2011.

[17] K. Alexis, G. Nikolakopoulos, A. Tzes, and L. Dritsas, "Coordination of Helicopter UAVs for Aerial Forest-Fire Surveillance," Appl. Intell. Control to Eng. Syst., pp. 169– 193, 2009.

[18] W. Krüll, R. Tobera, I. Willms, H. Essen, and N. Von Wahl, "Early forest fire detection and verification using optical smoke, gas and microwave sensors," *Procedia Eng.*, vol. 45, pp. 584–594, 2012.

[19] L. Merino, F. Caballero, J. R. Martínez-de Dios, J. Ferruz, and A. Ollero, "A cooperative perception system for multiple UAVs: Application to automatic detection of forest fires," *J. F. Robot.*, vol. 23, no. 3–4, pp. 165–184, 2006.

[20] D. W. Casbeer, D. B. Kingston, R. W. Beard, and T. W. Mc lain, "Cooperative forest fire surveillance using a team of small unmanned air vehicles," *Int. J. Syst. Sci.*, vol. 37, no. 6, pp. 351–360, 2006.

[21] H. X. Pham, H. M. La, D. Feil-Seifer, and M. Deans, "A distributed control framework for a team of unmanned aerial vehicles for dynamic wildfire tracking," in *IEEE International Conference on Intelligent Robots and Systems*, 2017, pp. 6648–6653.

[22] A. Ford and A. Roberts, "Colour Space Conversions," 1998..

[23] P. Gunjal, B. Gunjal, H. Shinde, S. Vanam, and S. Aher, "Moving Object Tracking Using Kalman Filter," in *International Conference On Advances in Communication and Computing Technology (ICACCT)*, 2018, pp. 544–547.

[24] G. Cai, B. Chen, and T. Lee, "Coordinate Systems and Transformations," in *Unmanned Rotorcraft Systems*, London: Springer, 2011, pp. 23–34.

[25] Mathworks, "Fundamental Coordinate System Concepts." .

[26] H. Vermeille, "An analytical method to transform geocentric into geodetic coordinates," J. Geod., vol. 85, pp. 105–117, 2011.

[27] DJI, "DJI-NAZA-M V2." .